Single-cell functional and chemosensitive profiling of combinatorial colorectal therapy in zebrafish xenografts

Rita Fior, Vanda Póvoa, Raquel Mendes, Tânia Carvalho, António Gomes, Nuno Figueiredo, Miguel Godinho Ferreira

Single cell functional and chemosensitive profiling of combinatorial colorectal therapy in zebrafish xenografts

Rita Fior[1], Vanda Póvoa[1], Raquel Mendes[1], Tânia Carvalho[2], António Gomes[3], Nuno Figueiredo[4], Miguel Godinho Ferreira[1]

[1]Fundação Champalimaud, [2]Instituto de Medicina Molecular, [3]Hospital Prof. Doutor Fernando Fonseca, [4]Champalimaud Foundation

Submitted to Proceedings of the National Academy of Sciences of the United States of America

Cancer is as unique as the person fighting it. With exception of few biomarker-driven therapies, patients go through rounds of trial-and-error approaches to find the best treatment. Using patient-derived cell lines, we show that zebrafish-larvae-xenotransplants constitute a fast and highly sensitive *in vivo* model for differential therapy response, with resolution to reveal intra-tumor functional cancer heterogeneity. We screened international colorectal cancer therapeutic guidelines and determined distinct functional tumor behaviors (proliferation, metastasis, angiogenesis) and differential sensitivities to standard therapy. We observed a general higher sensitivity to FOLFIRI than to FOLFOX, not only between isogenic tumors but also within the same tumor. We directly compared zebrafish-xenografts with mouse-xenografts and show that relative sensitivities obtained in zebrafish are maintained in the rodent model. Our data also illustrates how *KRAS* mutations can provide proliferation advantages in relation to $KRAS^{WT}$ and how chemotherapy can unbalance this advantage, selecting for a minor clone resistant to chemotherapy. Zebrafish-xenografts provide remarkable resolution to measure Cetuximab sensitivity. Finally, we demonstrate the feasibility of using primary patient samples to generate zebrafish Patient Derived Xenografts (zPDX) and provide proof-of-concept experiments that compare response to chemo and biological therapies between patients and zPDX. Altogether, our results suggest that zebrafish-larvae-xenografts constitute a promising fast assay for precision medicine, bridging the gap between genotype and phenotype in an *in vivo* setting.

zebrafish xenograft | chemotherapy-functional-screening | colorectal-cancer | KRAS | metastasis

INTRODUCTION

Chemotherapy regimens are developed and approved according to a demonstration of average efficacy and safety. However, efficacy rates are averages of individual responses. As result of this "one-size-fits-all" approach, treatments may prove to be successful for some patients but not for others. This is especially relevant in the metastatic scenario where oncology therapy guidelines reach branch points and clinicians face equivalent valid compounds i.e. with similar average response rates. Consequently, many patients go through inefficient treatments, being subjected to unnecessary toxicity.

The current gold standard in cancer biology for personalized screening is direct primary tumor transplantation into immune-compromised mice, also known as patient derived xenografts (PDX). PDXs can generally maintain both inter-individual and genetic heterogeneity of original tumors, mimicking disease responses in patients and thus reflecting the uniqueness of each patient (1). However, mouse PDXs present two major drawbacks for routine clinical assays: the amount of patient sample required and the time-frame for engraftment and expansion of colonies (months), rendering them unviable for clinical practice.

Zebrafish xenografts offer speed, cellular resolution and the ability to perform large numbers of transplants (2-4). They also allow evaluation of crucial hallmarks of cancer, such as metastatic (5-6) and angiogenic potentials (5, 7, 8). Even though drug pharmacodynamics in zebrafish may differ from mammals, many compounds have been shown to block disease in a similar way. This has led to an increasing amount of compounds discovered in zebrafish screens that are entering into human clinical trials (2-4). However, for zebrafish xenografts to be used as clinical assays, it is crucial that they provide sufficient resolution to reveal inter and intra-tumor functional heterogeneity, including differential response to therapy. Reliable methods to visualize and quantify human cells and induced cell death upon treatment and direct validation with mouse xenografts were also still lacking.

With the aim of testing zebrafish xenotransplants as a screening platform for cancer therapy, we used a panel of patient-derived human colorectal cancer (CRC) cell lines to screen the NCCN/ESMO treatment guidelines for advanced CRC. We selected independent cell lines to investigate inter-tumor heterogeneity and isogenic clones to examine intra-tumor heterogeneity. In just 4 days, we could detect *in vivo* differential behaviors with single cell resolution, namely differential proliferation rates, metastatic and angiogenic potentials. These differences were present not only in tumors derived from different patients but also between different clones from the same tumor, even when mixed into a polyclonal tumor. We showed that early read-outs of response to treatment in zebrafish closely mirror the results obtained in the mouse. We also found that the zebrafish xenograft

Significance

Despite advances in targeted cancer treatments, we still lack methods to predict how a specific cancer will respond to a given therapy. As a consequence, patients go through rounds of trial-and-error approaches based on guidelines to find the best treatment, often subjected to unnecessary toxicity. Using cell lines, we used zebrafish-larvae-xenografts as sensors for cancer behavior and therapy guideline screening. Our data not only shows sufficient resolution to distinguish functional tumor behaviors in just 4-days, but also differential sensitivity to colorectal cancer therapy. As proof-of-principle experiments, we provide evidence for similar behavior response to therapies in zebrafish patient derived xenografts. Altogether, our results suggest zebrafish-larvae-xenografts as a promising *in vivo* screening platform for precision medicine.

Figure 1

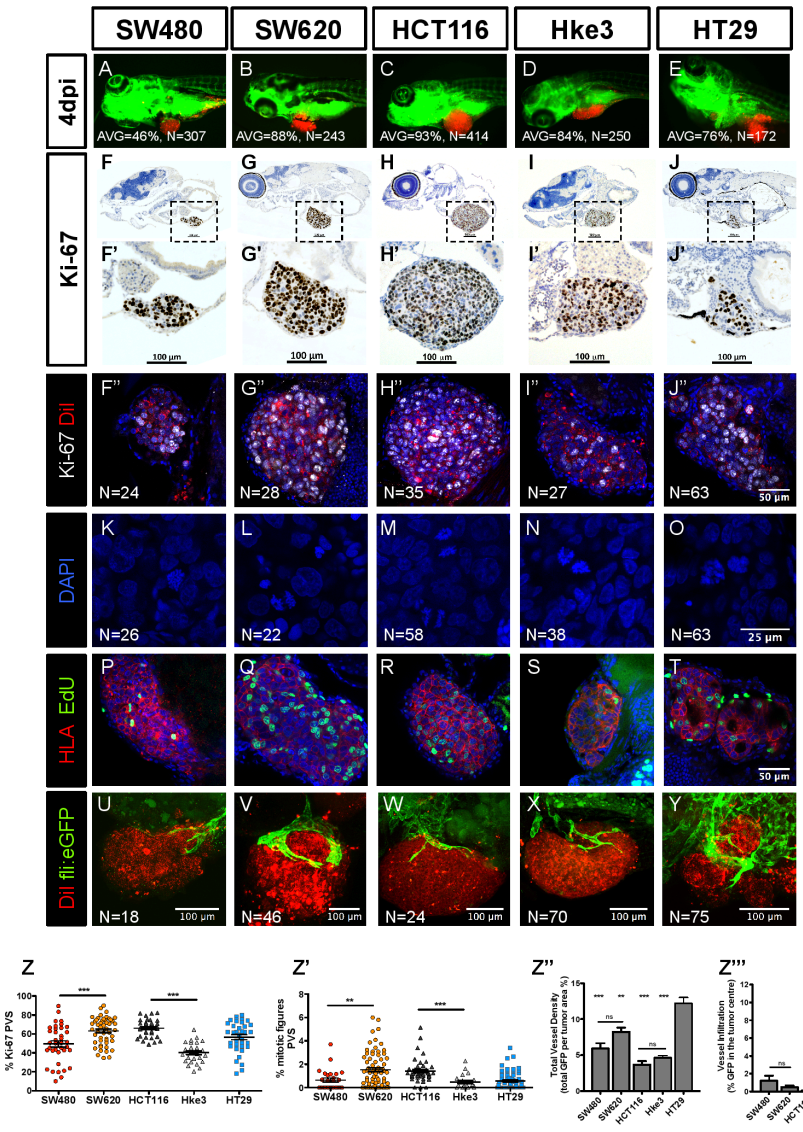

Fig. 1. | Implantation and histological analysis of human CRC zebrafish-xenografts. Human CRC cells (SW480; SW620; HCT116;Hke3and HT29) were labeled with the lipophilic CM-DiI dye (red) and injected into the PVS of 48hpf zebrafish. At 4dpi the number of xenografts with a tumor implanted was quantified (**a-e**), and the average (AVG) implantation rate was determined from at least 3 independent experiments. Immunohistochemistry for Ki-67 in paraffin sections at 4dpi xenografts (**f-j'**). Whole mount immunofluorescence staining at 4dpi, for Ki-67 (**f''-j''**), anti-human HLA in red and EdU staining in green (**P-T**). Representative images of mitotic figures in the corresponding xenografts (**K-O**), nuclei staining with DAPI in blue. Quantification of % of Ki-67 positive cells per xenograft (**Z,** p***<0.0001) and mitotic figures **Z'**, p***<0.0001) in corresponding tumors (each dot represents one xenograft). Human CRC xenografts were generated in Tg(fli:eGFP) zebrafish to visualize blood vessels. Images representative of 4dpi xenografts induced neovasculature: SW480 (**U**); SW620 (**V**); HCT116 (**W**); Hke3 (**X**)and HT29 xenografts (**Y**). Quantification of total vessel density (**Z**'') and vessel infiltration (**Z**'''), **|*** refers to comparison with HT29. HT29 tumors displayed significant higher vessel density and infiltration than any other tumor, SW480 vs HT29 p=0.0264; SW620 vs HT29 p=ns; HCT116 vs HT29 p<0.0001, Hke3 vs HT29 p<0.0001). Infiltration potential (SW480 vs HCT116 p=0.0482; SW480 vs HT29 p=0.0025; HCT116 vs HT29 p<0.0001). Results in **Z, Z',Z'',Z'''** are expressed as average (AVG) ± SEM. The number of xenografts analyzed for Ki-67, mitotic index and angiogenesis is indicated in the figures. All images in the same row are at the same magnification.

model revealed a remarkable sensitivity to detect differential responses to Cetuximab treatment according to the *KRAS* mutational status.

Finally, as a proof-of-principle, we generated CRC zebrafish PDX (zPDX) derived from surgery resected human samples and treated them with the same treatment administered to the patient. Future work will be aimed at validating this model in clinical studies to test predictability. Altogether, our results suggest that zebrafish xenografts are a fast and highly sensitive assay that can be used to display multiple biological tumor traits and assess tumor response to treatment. We propose that this model can be used, not only in the research setting, but also possibly in the future for precision medicine.

RESULTS

Human CRC display diverse implantation and proliferation potentials in zebrafish-xenografts

Our strategy relies on the ability of zebrafish xenotransplants to unravel inter and intra-tumor functional heterogeneity. To address this question, we selected several human CRC cell lines isolated from different patients (inter-tumor heterogeneity) and isogenic pairs (intra-tumor heterogeneity) described in Table S1. SW480 was derived from the primary tumor and SW620 from the lymph node metastasis (6 months later) of the same patient, illustrating a history of clonal selection (9). HCT116 $KRAS^{G13D}$ tumor cells were isolated from a patient with colorectal carcinoma. Hke3 cells were generated from HCT116 by a somatic deletion of the $KRAS^{G13D}$ allele, reverting the oncogenic KRAS phenotype (10). This pair is considered isogenic and constitutes an ideal setting to study phenotypic heterogeneity derived from one single mutation (intra-tumor heterogeneity). Finally, HT29 cells were isolated from a well-differentiated metastatic tumor, belonging to the goblet–like subtype (11), serving as an outgroup.

To determine the implantation potential of these 5 human CRC cell lines, cells were labeled with a lipophilic dye (DiI) and injected into the periviteline space (PVS) of 48 hours post fertilization (hpf) zebrafish embryos (8). At 4 days post injection (dpi), we scored the efficiency of implantation (Fig. 1a-e, Fig. S1). With exception of SW480 cells, we observed high implantation efficiency in all cell lines (>70%) (Figure S1).

Figure 2

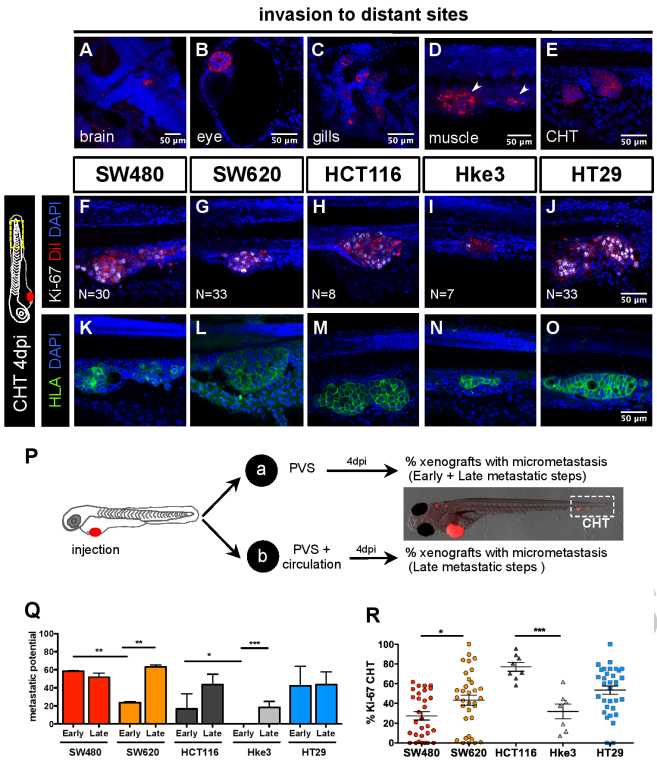

Fig. 2. | Human CRC cells show different metastatic potential. At 4dpi it is possible to detect human tumor cells throughout the zebrafish body, in the brain (**a**), eye (**b**), gills (**c**), muscle (**d**) and in the caudal hematopoietic tissue (CHT) (**e**). Immunofluorescence for Ki-67 (**f-j**) and anti-human HLA (**k-o**) in the CHT region at 4dpi in the indicated xenografts. In order to distinguish between early and late metastatic steps tumor cells were injected into the PVS only a) or in the PVS and directly into circulation b) (**p**). Quantification of Early (EMP) and Late (LMP) Metastatic Potential (**q**) and percentage of Ki-67 positive cells in the CHT micrometastasis (**r**, each dot represents one xenograft). Results are average from at least 3 independent experiments. The number of xenografts analyzed for Ki-67 is indicated in the images. The number of xenografts analyzed for EMP and LMP are as follows: SW480 (EMP N=62; LMP, N= 66); SW620 (EMP N=50, LMP N=69); HCT116 (EMP N=73, LMP, N=57); Hke3 (EMP N=74, LMP N=250; HT29 (EMP N=31, LMP N=94) (q). Results in **Q** and **R** are expressed as average (AVG) ± SEM. Nuclei staining with DAPI in blue. All pictures in the same row (**F-J**) are at the same magnification. All images anterior to the left, posterior to right, dorsal up, ventral down.

One of the most fundamental hallmarks of cancer is the capacity to proliferate with no constrains (12). To measure proliferation *in vivo*, we quantified mitotic figures and the Ki-67 index (specifically recognizes human cells, with no cross-reactivity with zebrafish) (Fig. 1f-j''). We found that the Ki-67 and mitotic index varied between cells derived from different patients (Fig. 1u, v). Direct comparison between isogenic pairs (intra-tumor heterogeneity) revealed that SW620 and HCT116 have higher proliferation rates in relation to their isogenic pairs SW480 (Ki-67 $p<0.0001$; mitosis $p=0.0063$) and Hke3 (Ki-67 $p<0.0001$; mitosis $p=0.0003$) (Fig. 1u, v). To further confirm that human CRC cells are actively proliferating in the zebrafish host, we delivered a 2h pulse of EdU prior fixation, labeling specifically cells that were undergoing DNA replication (Fig. 1p-t). edu incorporation demonstrates that human cells can actively proliferate in the zebrafish-xenograft model.

We also investigated whether the immunohistochemical profile and typical morphological features described for these cell lines were maintained in the zebrafish-xenografts (Fig. S2). As expected for more differentiated cells, HT29 formed tubular structures (Figure S2 E', O, T, T'), whereas tumors originating from the other cell lines showed a solid pattern with rare tubule formation, consistent with their "stem cell like" character (Fig. S2, 11).

We next examined angiogenesis, another essential hallmark of cancer (12). The 5 cancer cell lines were injected into Tg(fli:eGFP) zebrafish line with GFP labeled vasculature (13). At 4dpi, xenografts were imaged by confocal microscopy to study vessel 3D architecture (Fig. 1U-Y). SW480, SW620, HCT116 and Hke3 tumors showed a well-vascularized periphery, composed of large vessels that generally do not infiltrate the tumor (Fig. 1U-Y, Z''-Z''', MOVIES 2-5). In contrast, HT29 are highly vascularized tumors, with formation of a dense vessel network that infiltrates into the core of the tumor (Fig. 1Y, Z''-Z''' MOVIE_6 and 7). This is consistent with HT29 expressing high levels of VEGF and high angiogenic potential in other models (14,15).

Our data conclusively shows that human CRC cells can sustain proliferation in zebrafish and present different proliferation dynamics in CRC tumors derived from different patients and isogenic tumors. In addition, human CRC cells maintain their general cellular characteristics and angiogenic potential in the zebrafish-xenografts.

Isogenic human CRC cells present different metastatic potentials

Another essential hallmark of cancer is the ability of cells to form metastasis (12). At 4dpi, we could detect several small groups of cells in the brain, optic cup, gills, skeletal muscle and in the caudal hematopoietic tissue (CHT) region (Fig. 2 a-E). Cells in the CHT often extravasate from vessels (MOVIE1) and invade adjacent tissues, frequently the muscle (Fig. 2d, arrows). This "hot spot" region for tumor cell colonization provides an ideal location for quantification of metastatic potential (6). Immunofluorescence for HLA (anti-human MHC-class I subunit) identifies unequivocally cells of human origin and delineate the cellular architecture of the micrometastasis (Fig. 2k-o). Ki-67 positive cells and mitotic figures at 4dpi suggest that colonization has been achieved (Fig. 2f-j, r).

Metastatic efficiency may vary and depends on whether a tumor cell can detach from the primary tumor, enter and survive in circulation and go on to seed cells at distant sites. We designed a simple assay to distinguish between early-stages (invasion of surrounding tissues and intravasation into blood vessels) and later-stages of the metastatic cascade (survival in circulation, extravasation and colonization) (16,17) by comparing the micrometastasis efficiency when cells were placed directly into circulation vs when not. For that, we injected CRC cell lines either into the PVS alone (group_a) or directly into circulation (group_b) (Fig. 2p). At 4dpi, we analyzed the number of xenografts that presented a tumor cell mass (> 20 cells) away from the PVS injection site (CHT).

For tumor cells in group_a to efficiently establish metastasis, they would have to go through all the metastatic steps (from early to late steps) whereas cells in group_b only have to go through the later-stage ones. Thus, considering that maximum metastatic efficiency is achieved when cells are placed in circulation (group_b), the reduction of colonization in group_a would reflect the effort to undergo the early metastatic steps. Therefore, we converted our frequency of CHT colonization into Early Metastatic Potential (EMP) and Late Metastatic Potential (LMP) (Fig. 2p and methods).

Overall, our data shows that tumors differed both in their EMP (anova $p=0.0044$) and LMP (anova $p= 0.028$) (Fig. 2q). When comparing isogenic lines, we observed that SW480 cells have a higher EMP than SW620 ($p=0.004$) even though they exhibit similar LMP (Fig. 2q). These results agree with previous observations that SW480 cells are more invasive and migratory than SW620 *in vitro* and show higher extravasation potential *in vivo* (9, 18).

Figure 3

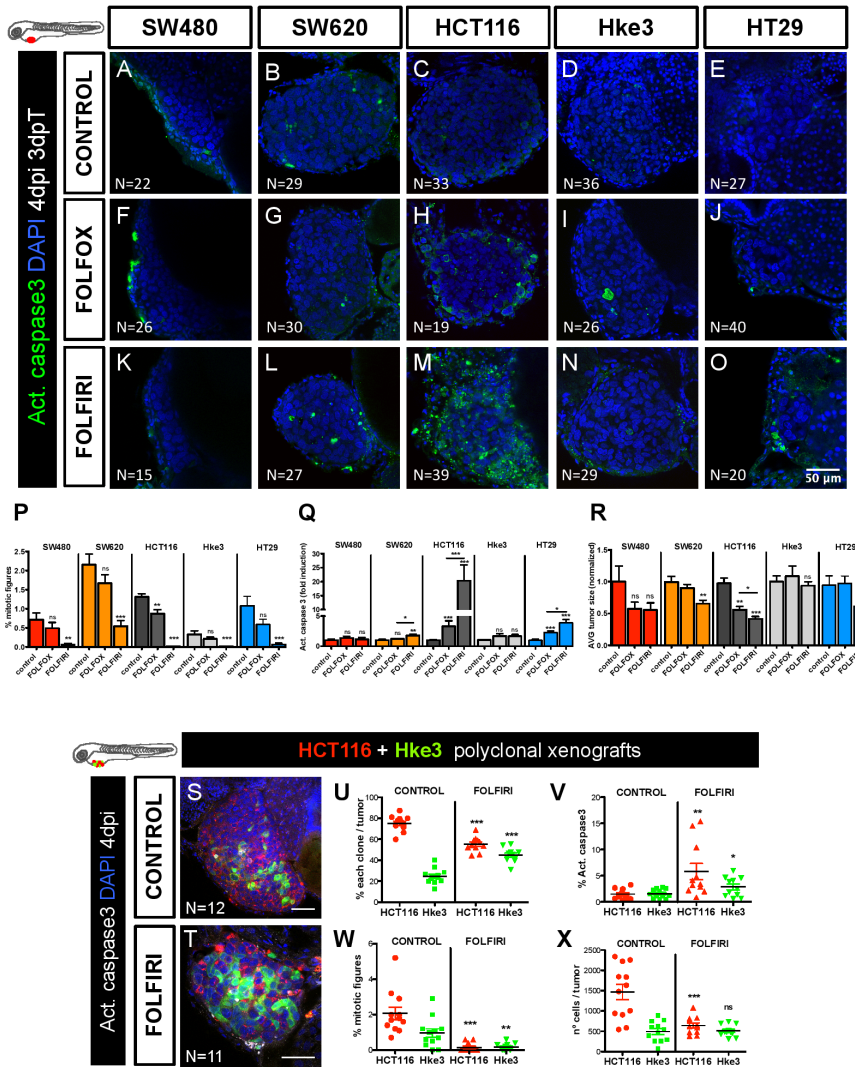

Fig. 3. | CRC xenografts show different sensitivity to standard chemotherapy. Human CRC zebrafish-xenografts were treated *in vivo* with FOLFOX (**f-j**) and FOLFIRI (**k-o**) compared to non-treated controls (**a-e**). Zebrafish were sacrificed and fixed at 4dpi, 3 days post treatment (3dpT). Mitotic index (**p**-DAPI in blue) and cell death by apoptosis (**q**-activated caspase3 in green) was analyzed and quantified. Average tumor size (number of DAPI cells) – normalized to respective controls was also quantified to compare between different xenografts in different conditions (**r**). All pictures are at the same magnification in the same row. Results in **p, q,**and **r**are expressed as average (AVG) ± SEM. Results are average from at least 3 independent experiments and the total number of xenografts analyzed is indicated in the images. ns - non significant, p values are indicated in the text, p***<0.001HCT116 and Hke3 polyclonal xenografts (1:1) were generated and randomly treated with FOLFIRI and compared to untreated controls. Xenografts were sacrificed and fixed at 4dpi, 3 days post treatment (3dpT). The % of each clone (**U**), cell death by apoptosis (**V**-activated caspase3), mitotic index (**W**) and the size of each clone per xenograft (**X**), was analyzed and quantified. Each dot represents a xenograft, Hke3_caspase3 p**=0.041, Hke3_mitosis p**=0.006, remaining p values are indicated in the text, p***<0.001. The total number of xenografts analyzed is indicated in the images. HCT116 was labeled CM-DiI (red) and Hke3 with the lipophilic dye DeepRed (green –false colour).

The isogenic pair HCT116 / Hke3 showed different EMP (Fig. 2h, i, q, p***<0.0001) ie in Hke3 *KRAS*^{WT} xenografts, we could only find metastasis when cells were directly injected into circulation (Fig. 2i, n, q, p<0.0001), highlighting the reported roles for activated KRAS in early metastatic events (17,18,20).

Finally, HT29 cells showed high EMP and LMP, frequently forming organized masses in the eye and CHT (Fig. 2 a, j, o, q). This high metastatic potential is consistent with the one observed in mouse xenograft models (19).

Our results show that is possible to further discriminate the cellular metastatic potential by comparing the efficiency of cells to metastasize when placed directly into circulation or not. Importantly, we found that the measurement of metastatic potential in our model match the previously described.

Zebrafish-xenografts discriminate different chemosensitivities in 4 days

To test whether zebrafish-xenografts can measure responses to therapy, we first assessed the main therapeutic options in advanced CRC guidelines: FOLFOX (5-FU+Oxaliplatin+Folinic acid) and FOLFIRI (5-FU+Irinotecan+Folinic acid) (Table S2, 20). These protocols are considered as balanced alternatives, since both treatments have shown equivalent average response rates (~35%) in clinical trials performed on naïve patients (21).

To assess chemotherapeutic responses, all xenografts were randomly distributed between treatment groups (control, FOLFOX and FOLFIRI) at 24hpi and then treated for 3 consecutive days. An average of 30 xenografts were treated per condition. Compounds were delivered directly in the embryo medium and replaced daily. After three days of treatment (and 4dpi), xenografts were processed for microscopy and assessed for mitotic index, cell death by apoptosis (activated Caspase 3) and tumor size (Fig. 3p,q, r).

FOLFIRI treatment induced a significant reduction of mitotic figures in all tumors (Fig. 3p). However, a significant induction of apoptosis followed by a reduction of tumor mass was only observed in HCT116 (apoptosis p<0.0001; 59% tumor reduction p<0.0001) and SW620 (apoptosis p=0.0021; 35% tumor reduction p=0.0026) (Fig. 3l, m, q, R). Remarkably, SW620 and HCT116 are more sensitive than their respective isogenic pairs. These results suggest differential sensitivities to therapy throughout cancer progression (primary vs metastasis) and in heterogeneous tumor populations (*KRAS* subclones).

Only in HCT116, FOLFOX treatment resulted in significant induction of apoptosis accompanied by a reduction of tumor size (apoptosis p<0.0001; 44% reduction p=0.0018) (Fig. 3h, q, r). Strikingly, Hke3 (HCT116 isogenic pair), showed no induction of

Figure 4

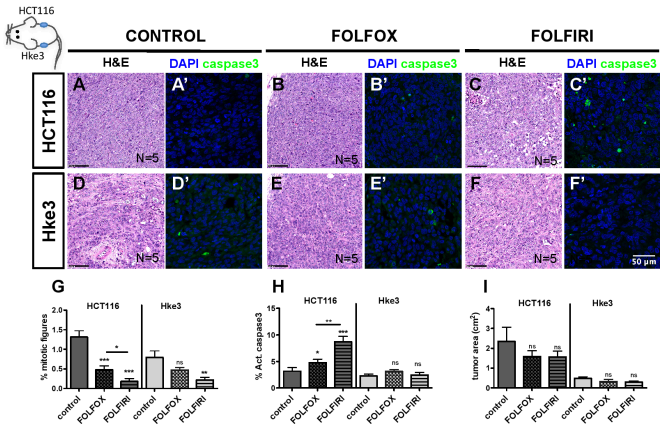

Fig. 4. | HCT116 and Hke3 mouse xenografts validate zebrafish chemosensitive profileHCT116 and Hke3 double mouse xenografts were generated and randomly treated with FOLFOX (N=5) and FOLFIRI (N=5) and compared to PBS treated controls (N=5). Hematoxilin and Eosin (H&E) (**a-f**) staining as well as immunofluorescence to detectapoptotic cells (activated caspase3, **a'-f'**) was performed in paraffin sections. Mitotic index (**g**-DAPI in blue) and cell death by apoptosis (**h**-activated caspase3 in green) was quantified in fields distant from the necrotic center of the tumor. ns - non-significant, p values are indicated in the text, p***<0.001. Results in **g** and **h** are expressed as average (AVG) ± SEM.

Figure 5

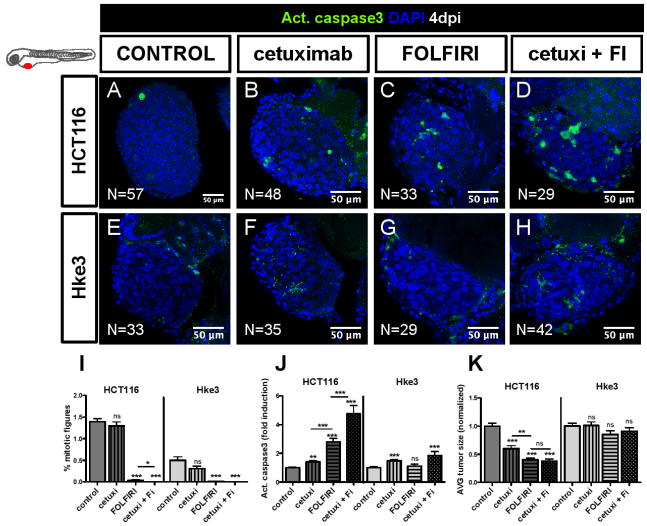

Fig. 5. | Differential sensitivity to Cetuximab in human CRC in zebrafish-xenograftsHCT116 (**a-d**) and Hke3 (**e-h**) xenografts were treated for 3 consecutive days, with Cetuximab (**b, f**), FOLFIRI (**c, g**) and Cetuximab in combination with FOLFIRI (cetuxi + FI, **d, h**) and compared to control non-treated xenografts (**a, e**). Mitotic index (**i**-DAPI in blue), cell death by apoptosis (**J**-activated caspase3 in green), and average (AVG) tumor size (**k**-number of DAPI cells per tumor) was analyzed and quantified at 4dpi and 3dpT. Average tumor size and the % of activated caspase3 was normalized to respective controls to compare between different xenografts. Results are expressed as average (AVG) ± SEM. All images anterior to the left, posterior to right, dorsal up, ventral down.

apoptosis or reduction of tumor mass when treated with FOLFOX (Fig. 3i, q, r). These results are consistent with KRAS mutations increasing sensitivity to 5-FU induced apoptosis (22). As for HT29, as previously reported in mouse xenografts (23), we could observe a significant reduction of mitotic figures ($p<0.0001$) and increase in apoptosis both upon FOLFIRI ($p<0.0001$) and FOLFOX treatment ($p<0.0001$) (Fig. 3P, Q).

In general, our results are consistent to previous mouse *in vivo* studies (24, 25) with exception of SW620, which has been reported to respond to FOLFOX (25). The differences observed in our study are likely to reflect that our assay is designed to detect fast strong responses, given its short time window (3 days). This is particular evident in the study by Van Schaeybroeck (26) where HCT116 tumors stop growing as soon as FOLFOX treatment is initiated, whereas SW620 shows a delayed response.

In summary, we show that zebrafish-larvae-xenografts have enough resolution to measure inter-patient and intra-patient heterogeneity chemotherapy responses in just 4 days. These results highlight the heterogeneity of chemotherapeutic response and the possibility to measure this in a very short period of time *in vivo*.

To further confirm the HCT116 ($KRAS^{MUT}$) and Hke3 ($KRAS^{WT}$) opposing chemosensitive profiles we challenged them in the same xenograft host. For that, we co-injected the 2 cell lines (1:1), each labeled with a different lipophilic dye. Mixed xenografts (HCT116+Hke3) were randomly distributed into FOLFIRI and control groups. As expected, given their higher proliferative potential, HCT116 $KRAS^{MUT}$ cells outcompete Hke3 $KRAS^{WT}$ and become dominant in the mix, representing ~80% of the tumor (Fig. 3S-S',U). However, upon FOLFIRI treatment, HCT116 significantly reduced its frequency ($p<0.0001$) (Fig. 3U). Consistent with the individual response to FOLFIRI treatment, we observed a significant increase in apoptosis ($p=0.0023$), a decrease in mitotic figures ($p<0.0001$) accompanied by a significant decrease in HCT116 tumor size (~56% reduction $p<0.0001$) (Fig. 3V-X). In contrast, Hke3 clone size did not change upon FOLFIRI treatment, remaining at similar levels to controls (Fig. 3V-X).

These results demonstrate the differential chemosensitive profiles of both cell lines and how the KRAS mutation sensitizes cells to chemotherapy (25, 27). Our data also illustrate how in heterogeneous tumors, KRAS mutations can provide a proliferation benefit, and how chemotherapy may disrupt this advantage, selecting the minor clone resistant to treatment, which then maybe responsible for relapses.

HCT116 and Hke3 NOD-SCID mouse xenografts show similar chemosensitive profile to zebrafish-xenografts

To directly compare the HCT116 and Hke3 chemosensitive profile determined in zebrafish with mouse xenografts, we generated HCT116/Hke3 double mouse NOD-SCID xenografts, controlling treatment efficacy and delivery in the same animal (28). After 14 days, mice were randomly distributed amongst treatment groups and treated with 3 cycles of chemotherapy (Fig. 4).

Similarly, to our zebrafish-xenograft results, Hke3 mouse tumors presented a reduced mitotic index upon FOLFIRI treatment but not with FOLFOX (Fig. 4D-F', G) and no significant difference in apoptosis was observed with both treatments (Fig. 4H). Also in agreement to what we observed in zebrafish, both FOLFOX and FOLFIRI induced a significant increase in apoptosis in HCT116 cells (Fig. 4a'-c', H) and reduced proliferation (Fig. 4H, G) albeit FOLFOX to a minor extent than FOLFIRI (FOLFOX vs FOLFIRI: apoptosis $p=0.0017$, mitotic figures $p=0.029$), closely resembling the zebrafish results (Fig. 3P,Q).

However, we were unable to detect clear differences in tumor size between control and treatment groups in our mouse xenograft study (Fig. 4). This contrasts not only to our zebrafish-xenograft results (Fig. 3R) but also to previous mouse studies, where FOLFOX reduces the size of HCT116 tumors (26). The inability to detect tumor reduction in mouse xenografts is likely to rely on different experimental designs (treatment initiation-3 days vs 14 days post inoculation) that may lead to different

Figure 6

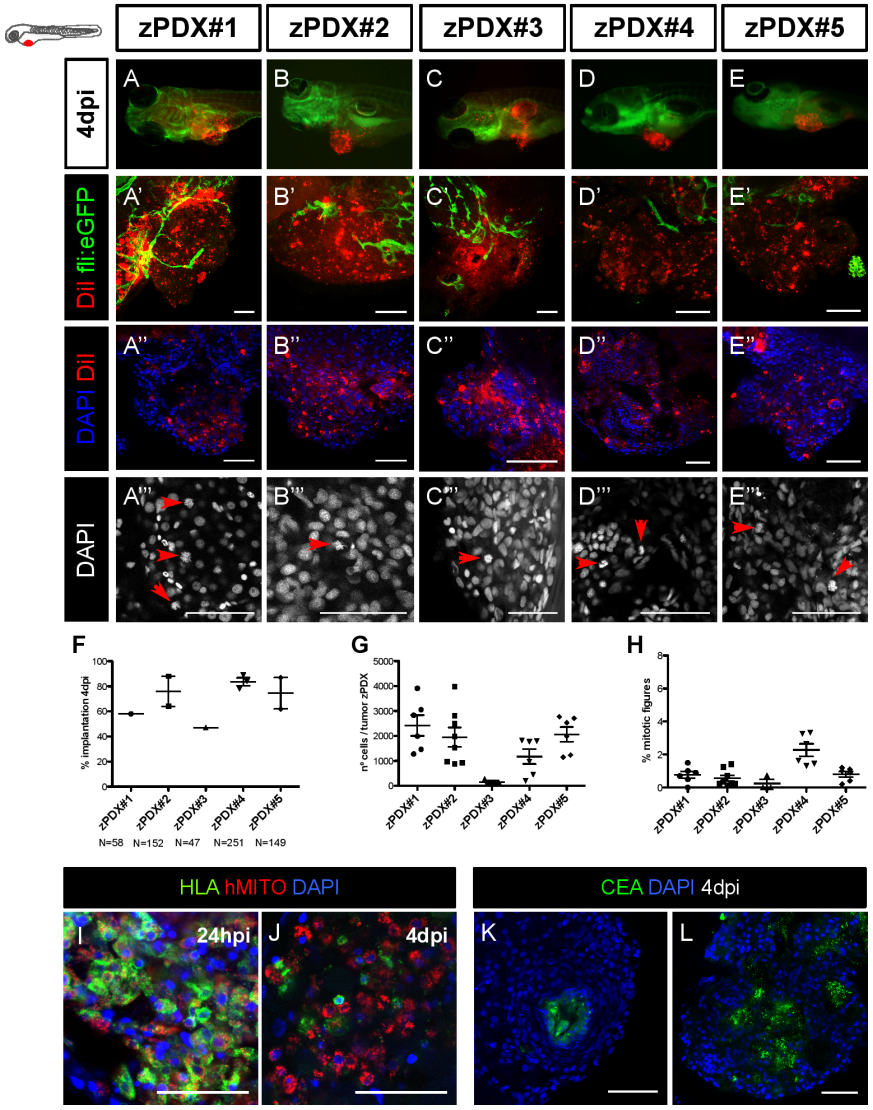

Fig. 6. | Zebrafish patient-derived xenografts (zPDX) can be efficiently established using human colorectal cancer primary samples Cell suspensions derived from surgically resected human colon tumors were labeled with the lipophilic CM-DiI dye (red) and injected into the PVS of 48hpf wt or Tg(fli:EGFP). At 4dpi the number of zebrafish with an implanted tumor was quantified (**A-E, F,** each dot represents implantation % of each experiment). Representative confocal images of 4dpi zPDX showing neovasculature in Tg (fli:EGFP) (**A'-E'**) and tumor masses with high cytomorphologic and architectural diversity (DAPI **A''-E''**). The number of nuclei (tumor size, **G**) and mitotic figures (**H**) in these tumor masses was quantified (**G**) each dot represents one xenograft Representative images of mitotic figures (**A'''-E'''**, red arrows) and corresponding quantification (**H**). HLA and human mitochondria-immunostained cells at 24hpi (**I**) and 4dpi (**J**). Tubular structures with luminal CEA staining (**K, L**). All images anterior to the left, posterior to right, dorsal up, ventral down. Scale bar, 50µm.

tumor growth kinetics. Thus, with exception of long-term tumor size decline, our results in mouse xenografts show higher response to treatment in HCT116 than in Hke3 cells, closely matching zebrafish-xenografts.

Differential sensitivity to Cetuximab and Regorafinib in CRC tumors in zebrafish-xenografts

Our results suggest that Hke3 $KRAS^{WT}$ tumors were refractory to FOLFOX and FOLFIRI standard chemotherapy. CRC guidelines further recommend that $KRAS^{WT}$ patients should be treated with a combination of chemotherapy and Cetuximab, a monoclonal antibody anti-EGFR (26). $KRAS^{WT}$ status is an established biomarker for Cetuximab treatment (20, 27). Consequently, patients with metastatic CRC who present a mutated *KRAS* profile ($KRAS^{MUT}$), such as in HCT116, are generally excluded from Cetuximab treatment (21).

To test whether Cetuximab therapy could induce cell death and reduce tumor mass in Hke3 tumors, we treated Hke3 $KRAS^{WT}$ and HCT116 $KRAS^{MUT}$ xenografts (as a negative control) with Cetuximab, FOLFIRI and with a combination of FOLFIRI with Cetuximab. Surprisingly, Cetuximab alone could significantly induce apoptosis both in Hke3 and HCT116 tumors (Fig. 5b, f, j). Combination of Cetuximab with FOLFIRI resulted in increased sensitivity of individual treatments in HCT116 tumors (Fig. 5d, H, j). This synergistic effect was also observed in the reduction of mitotic figures, but not in the reduction of tumor size (Fig. 5i, k).

We were surprised to observe the effect of Cetuximab in HCT116 (Fig. 5i, j, k), given the status of $KRAS^{MUT}$. However, it was recently reported that a proportion of patients with $KRAS^{G13D}$ mutations, but not with $KRAS^{G12V}$ mutations, benefit from treatment with Cetuximab (28). Thus, to further test the sensitivity of our *in vivo* assay, we treated SW620 $KRAS^{G12V}$ tumors with Cetuximab (Fig. S3 E, F, G). In contrast to HCT116 $KRAS^{G13D}$, but as expected for $KRAS^{G12V}$ tumors, no significant effect was observed with Cetuximab treatment in SW620 $KRAS^{G12V}$ tumors (Fig. S3). These results demonstrate that the zebrafish-xenograft assay has a remarkable resolution to detect sensitivity to Cetuximab treatment, even in $KRAS^{G13D}$ tumors.

Although Cetuximab treatment of Hke3 $KRAS^{WT}$ tumors induced apoptosis, this was not accompanied by a significant

Figure 7

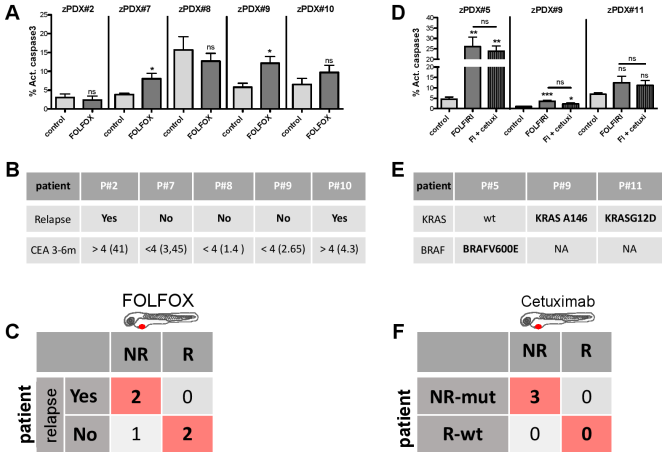

B

patient	P#2	P#7	P#8	P#9	P#10
Relapse	Yes	No	No	No	Yes
CEA 3-6m	> 4 (41)	<4 (3,45)	< 4 (1.4)	< 4 (2.65)	> 4 (4.3)

E

patient	P#5	P#9	P#11
KRAS	wt	KRAS A146	KRASG12D
BRAF	BRAFV600E	NA	NA

C — FOLFOX

patient relapse	NR	R
Yes	2	0
No	1	2

F — Cetuximab

patient	NR	R
NR-mut	3	0
R-wt	0	0

Fig. 7. | zPDX treatment response may predict relapse and correlate with known genomic biomarkers of Cetuximab resistance5 zPDX corresponding to patients subjected to curative surgery and postoperative FOLFOX adjuvant treatment, were treated with FOLFOX for 3 days and processed for immunofluorescence. Cell death by apoptosis (**A**-activated Caspase3) was analyzed and quantified. zPDX#7 control vs FOLFOX p=0.037; zPDX#9 control vs FOLFOX p=0.016.**B.** Relapse and CEA levels information of the 5 patients analyzed. (**C**). Confusion matrix displays the number of patients with actual and predicted responses in zPDX ie responders are patients that did not relapse (R) and patients that relapse are the non-responders (NR). **D.** 3 zPDX were treated with FOLFIRI and FOLFIRI in combination with Cetuximab, cell death by apoptosis (activated Caspase3) was analyzed. zPDX#5 control vs FOLFIRI p=0.0043, control vs FOLFIRI+Cetuximab p=0.0084; zPDX#9 control vs FOLFIRI p=0.001, control vs FOLFIRI+Cetuximab p=0.012.**E.** Genomic information of the analyzed patients. **E.** Confusion matrix displays the number of patients with mutations predicted of resistance with predicted responses in zPDX.

reduction of tumor mass (Fig. 5I, k), suggesting that Cetuximab, is not very effective in Hke3 cells.

Regorafenib is a small molecule multikinase inhibitor recommended in refractory metastatic CRC, usually used as last alternative in the guidelines (20, 29). Regorafenib not only has been shown to induce apoptosis (24) but also to have anti-angiogenic activity (29). Thus, to test whether Regorafinib could be more effective for Hke3 refractory and less proliferative tumors, xenografts were treated with Regorafinib for 3 consecutive days. Although we could not observe changes in the mitotic index of Hke3 (Fig. S4F), Regorafinib was able to induce apoptosis in Hke3 cells ($p<0.0001$) accompanied by a significant reduction of tumor size (Fig. S4 A,B,G, H $p= 0.0041$). These results highlight the possibility to detect response to therapy even in low proliferative and refractory tumors.

In addition, since Regorafinib is also considered anti-angiogenic, we also examined this effect in HT29 xenografts (which we previously shown were highly angiogenic). We detected a reduction on the total vessel density in HT29 tumors (Fig. S4I C',D' $p<0.0001$) but not in Hke3 or SW620 (Fig. S4I, A', B', E', F'). Regorafinib also induces apoptosis in HT29 tumors, however this induction is not accompanied by a reduction of tumor mass as in Hke3 (Fig. S4G, $p=0.0083$, H). These results suggest that Regorafinib is efficient as a 3rd line of treatment for Hke3 refractory tumors and that Regorafenib is also able to block tumor derived neovascularization in highly angiogenic tumors.

Overall, we show that it is possible to perform an *in vivo* screening of the main current options of the international CRC treatment guidelines from 1st to 3rd line, by utilizing the zebrafish-larvae-xenograft model.

Zebrafish patient-derived xenografts (zPDX) can be efficiently established using human colorectal cancer primary samples

Next, to test whether zebrafish-larvae can be efficiently used to generate patient derived xenografts (zPDX), we injected cell suspensions derived from surgically resected human colon tumors into zebrafish. We developed a protocol based on procedures for human CRC organoids derivation to maintain stemness and cell viability during processing (30, 31) (SI text).

Selected primary tumors corresponded to adenocarcinomas of diverse tumor stage (Table S3). 24hpi zPDX were selected for the presence of a DiI stained mass in the PVS and left to develop for 3 more days. At 4dpi, percentage of implantation was scored as previously (Fig. 6F). We observed implantation rates ranging from 47% (zPDX#3) to 89% (zPDX#4) (Fig. 6F, A-E). For large primary tumor samples (zPDX#2, zPDX#4 and zPDX#5), injections were repeated and gave rise to similar engraftment rates (Fig. 6F), demonstrating the reproducibility of the procedure.

zPDXs were processed for whole mount immunofluorescence to assess angiogenesis (Fig. 6A'-E'), tumor size (Fig. 6G), mitotic figures (Fig. 6H), expression of colorectal cancer markers (carcinoembryonic antigen, CEA) and human-associated antigens (MHC-classI - HLA and human mitochondria) (Fig. 6I-L). Confocal microscopy analysis allowed us to observe differential vessel recruitment (Fig. 6A'-E') and tumor masses with high cytomorphologic and architectural diversity (Fig. 6A"-E"). Interestingly, even tumors with low cellularity induced vessel recruitment (Fig. 6C', G). Mitotic figures were present at 4dpi in all zPDX analyzed, albeit sparse and with low mitotic index (Fig. 6A"'-E"', H). We observed tubular structures with luminal CEA staining (Fig. 6K, L) as well as human HLA (to variable levels) and human mitochondria stained cells (Fig. 6I, J). We also compared directly the zPDX histology with the parental primary tumors with H&E (Fig. S5). zPDX derived from these tumors generally conserved their original features. They formed multilocular mucin lakes (Fig. S5A", B", C"), black dash lines delineate mucin lakes and red arrow heads for mucin), circumscribed by epithelium arranged as acinar structures with strips of cells or single cells (Fig. S5 A", A"', C", red dashed lines). Periodic acid-Schiff plus diastase (PAS+D) staining was used to identify mucus in the lumen of these structures (Fig. S6). Glandular structures accumulating necrotic debris in the lumen were also frequently seen (Fig. S5 A", B", black arrow heads), often CEA positive (Figure 6K).

Comparison of zPDX drug treatment with short-term patient treatment responses

In order to test our model as a platform to study response to treatment, we used available surgically resected CRC samples derived from patients that were subjected to FOLFOX adjuvant chemotherapy to reduce risk of disease relapse. At the time of initial diagnosis, almost two-thirds of patients with CRC undergo resection with curative intent. However, 30%-50% of these patients relapse and die of their disease. The majority of these recurrences occur during the first 2 years after surgery and most follow-up programs end 5 years after the primary treatment (32). FOLFOX postoperative adjuvant treatment has been shown to reduce chances of relapse improving disease-free survival (33).

Although not the ideal setting to study predictability, we sought to test if response to FOLFOX treatment in zPDX would anticipate a delay in relapse in the matching patients, or whether resistance to drug treatment in our model would associate with tumor relapse.

We generated zPDX from 5 different tumors and treated them with FOLFOX over 3 days. In the 5 zPDX, we could only observe response to FOLFOX treatment (induction of activated caspase3) in 2 zPDX (Fig. 7A & Fig. S7). These zPDX correspond

to patients in which, at 6 months after surgery, the levels of CEA remain stable, with no indication of relapse. In contrast, of the 3 zPDX which we could not detect response to FOLFOX treatment, 2 are already in relapse after 3 months, with increasing levels of CEA and clinical evidence of recurrence (Fig. 7A, B & Fig. S7). Thus, we could anticipate relapse / no relapse within 3-6m after surgery in 4 out of 5 patients.

Our previous results on the sensitivity to Cetuximab treatment to detect responses in tumors with $KRAS^{G13D}$ mutations prompted us to test whether response to Cetuximab in zPDX would correlate with genomic prediction of response to the EGFR blocking therapy. As a proof of concept, in order to test this assumption, we treated 3 zPDX with a combination of FOLFIRI with Cetuximab and FOLFIRI alone. In the 3 zPDX generated, we could observe no added effect of Cetuximab in combination with FOLFIRI, suggesting that the 3 tumors tested showed resistance to Cetuximab (Fig. 7D, Fig. S7F-H''). We later sequenced the corresponding tumors and observed that all harbored mutations on either KRAS or BRAF (Fig. 7E). All these mutations highly correlated to resistance to Cetuximab (34). Thus, our results corroborated the genomic prediction (Fig. 7F).

Even though we have not yet gathered sufficient patient numbers to reach statistical significance, we performed proof-of-concept experiments to set the ground for a future clinical study to test the predictiveness of zPDX in the more suitable neoadjuvant setting.

DISCUSSION

Recent genome cancer profile studies exposed unanticipated tumor heterogeneity. This heterogeneity has been observed not only between cancers (inter-tumor), but also within each cancer (intra-tumor) (35, 36). Even identical CRC clones that share the same genome exhibit multiple functional profiles (including distinct responses to therapies) (37), implying that the basis for heterogeneity is not only genetic. Most approved drugs lack known biomarkers and, even in biomarker-driven therapies, response rates are not full proof (36, 38). Thus in the current scenario, we are currently unable to securely forecast which patient is likely to respond to a given therapy program.

Chemosensitivity tests are not a novel idea. However, the accuracy of in vitro tests has not been robust enough to support its use in oncology practice (39). Recently, Letai and colleagues (40) showed a promising in vitro assay that bypasses serial passages and directly challenges tumor cells with therapeutic drugs, using BH3 profiling as a proxy of cell death. In this assay, there is a direct measurement of mitochondrial stress upon the applied drug (40, 41). In addition, in vitro organoids constitute a major technological breakthrough to study tumor biology, drug discovery and possibly also for personalized medicine (42).

Although promising, *in vitro* tests will always lack the complexity of interactions of tumor cells with its microenvironment in the *in vivo* setting. The current gold standard for in vivo assessment of tumor heterogeneity and response to therapy are mouse PDX (1). However, mouse PDX are not practical for clinical advice due to the time it takes to implant tumors, expand colonies and costs they entail. Here, we have taken an intermediate approach – a fast *in vivo* assay with unprecedented cellular resolution - the zebrafish-larvae-xenograft model.

We set out to test whether the zebrafish-larvae-xenografts have enough resolution to uncover functional cancer heterogeneity to screen *in vivo* international treatment guidelines. Our study shows that zebrafish-xenografts are capable to discriminate, with single cell resolution, distinct proliferation dynamics and differential metastatic potentials, not only between tumors derived from different patients but also between isogenic pairs.

Our ultimate goal was to screen the major therapeutic options present in the international guidelines for advanced CRC (20) using the zebrafish-xenograft assay. We analyzed the response of 5 zebrafish-xenografts (cell-line-derived) to the 2 most common and equivalent chemotherapy options FOLFOX and FOLFIRI (21) and observed an overall higher sensitivity to FOLFIRI than to FOLFOX. This is in agreement with the study by Sadanandan et al (11) that found that 70% of stem-like subtype tumors were associated with a clinical benefit with FOLFIRI treatment. Remarkably, we could also observe a clear differential response to therapy between isogenic tumors, illustrating differential therapy responses between primary and metastatic tumors (SW480/SW620) and subclonal tumor populations (HCT116/Hke3). We also reproduced polyclonal tumor scenarios and show differential responses to chemotherapy in the same xenograft and how therapy can select for minor resistant clones.

Following the next recommended therapy in the guidelines, we tested for Cetuximab sensitivity. Cetuximab treatment is a biomarker-driven therapy, recommended specifically for KRASWT tumors. Although not effective in all patients with KRASWT tumors (only ~12.8%), the probability of response to Cetuximab treatment is still significantly higher (25). To our surprise, Cetuximab was effective on HCT116 KRASG13D. Consistent with our results, recent clinical reports revealed that a significant portion of patients with KRASG13D mutations, but not KRASG12V, benefit from Cetuximab treatment (27). Thus, our results suggest that zebrafish-xenografts can measure responsiveness to therapy of tumors with different KRAS point mutations. Our study also illustrates the relevance of functional assays even in biomarker-driven therapies to further select the patients that may benefit from specific therapies, specifically in ones that do not have 100% efficacy and are expensive or toxic.

Although Hke3 $KRAS^{WT}$ tumors responded to Cetuximab treatment this was not accompanied by a reduction of tumor size. Thus, we tested the 3rd-line option for refractory metastatic CRC – Regorafenib. In contrast to previous treatments, Hke3 tumors now responded to therapy with an induction of apoptosis accompanied by reduction of tumor size. Our results illustrate the possibility to screen treatment guidelines from 1st to 3rd line.

We also validated our results obtained in zebrafish in NOD-SCID mouse xenografts. This is the first study to directly compare zebrafish vs mouse xenografts chemosensitivity. As in zebrafish, HCT116 responded to both treatments, but FOLFIRI produced a significant higher induction of apoptosis than FOLFOX and Hke3 seemed refractory to both treatments. Our results suggest that, using apoptosis and reduction of mitotic index as surrogate as response to treatment in zebrafish-xenografts (4 days from injection to analysis) can be used as proxy of the response to treatment in mouse xenografts (minimal 1 month since injection to analysis). The disparity in time between models is likely to reflect the difference in scale of the models (>10,000 fold). On the one hand zebrafish-larvae allow for visualization of single cells and their response to treatment in multiple xenografts, improving statistical power. In contrast, mouse PDXs generally rely on large palpable tumors, long treatments to visualize responses and multiple rounds of expansion to provide statistical power. On the other hand, this longer assay permits the study of tumor evolution, emergence of resistance clones and overall progression of disease (1, 37). Thus, we envisage that zebrafish and mouse xenografts models may complement each other: zebrafish as a fast screening platform, and mouse xenografts to accompany tumor evolution and relapse.

Lastly, we also demonstrate feasibility of using primary patient samples to generate zPDX with similar implantation rates as tumor cell lines. We show that zPDX can form tumor masses, induce vascularization and present multilocular mucin lakes, glandular structures and CEA expression. As observed with cell lines (SW480), patient samples (e.g. zPDX#3) also vary in their

engraftment efficiency (being as low as <50%). To overcome possible low implantation rates, we may increase the number of injected fish and use immune compromised strains (43, 44) to dampen the possibility of rejection. As a proof of concept experiments, we also treated zPDX with FOLFOX and were able to anticipate relapse / no-relapse within 3-6m after surgery in 4 out of 5 patients. In addition, we sequenced tumors whose matching zPDX did not responded to Cetuximab, and found that all harbored mutations highly linked to Cetuximab resistance, corroborating our zPDX results with genomic data.

In summary, we performed proof-of-concept experiments that show that it is possible to screen the available therapeutic options present in the international CRC guidelines by using zebrafish-xenografts. We show that zebrafish-larvae-xenografts constitute a rapid model with high sensitivity to unravel human tumor functional heterogeneity. We also performed proof-of-concept experiments using patient samples to set the ground for a clinical study to test the predictiveness of zPDX as a rapid *in vivo* screening platform for personalized cancer treatments.

Material and Methods

Animal care and handling

Zebrafish (Danio rerio) casper, casper; Tg(fli1:eGFP), nacre fish were handled according to European animal welfare regulations and standard protocols.

Human tissue

All samples used for zebrafish patient derived xenografts (zPDX) establishment were obtained from Champalimaud Hospital or Prof. Doutor Fernando Fonseca Hospital with written informed consent. The study was approved by the Ethics Committees of both Hospitals.

Cell lines and culture

Colon cancer cell lines, SW480, SW620 and HT29, originally from American Type Culture Collection (ATCC) were authenticated through short tandem repeat (STR) profiling karyotyping isoenzyme analysis. HCT116 and Hke3 isogenic cell lines were donated by Angela Relógio and analysed. All cells lines were tested for mycoplasma. All cells were cultured in DMEM (Biowest) supplemented with 10% fetal bovine serum (FBS - Biochrom) and 1% Penicillin-Streptomycin (Hyclone) in a humidified atmosphere containing 5% CO2 at 37ºC.

Zebrafish-Xenografts injection

Dil labeled cells were injected into the periviteline space (PVS) of anesthetized 48hpf larvae (**12**). After injection, xenografts were transferred to 34ºC until the end of experiments.

Zebrafish-Xenograft Drug administration

24hpi, zebrafish-xenografts with same tumor size were randomly distributed in the treatment groups: control E3 medium, FOLFIRI in E3 and FOLFOX in E3 (4.2 mM 5-FU, 0.18mM Folinic Acid, 0.08mM Irinotecan, 0.08mM Oxaliplatin) for 3 consecutive days. Using as a reference the maximum patient's plasma concentration of each compound (Table S2), we determined the zebrafish maximum tolerated concentration. Cetuximab monoclonal antibody was added to the cell suspension (20mgml) at the time of injection and then to E3 medium at 100mg ml. Regorafinib was added to E3 to a final concentration of 40mM .

Acknowledgements

We would like to thank the Champalimaud Histopathology Unit (Dr. A. Beltran, L. G. Madruga and M. Castillo) and Hospital Prof. Doutor Fernando Fonseca, for immunohistochemistry and pathology support. Surgery Units of Champalimaud Foundation (Dr. J.F. Cunha) and Hospital Prof. Doutor Fernando Fonseca (Dr. V. Nunes, Surgery Unit B) for patient samples. Champalimaud Fish and Rodents Facility (C. Certal, S. Mello) and IGC Fish Facility for excellent animal care. We also thank the IGC and IMM histology units. We also thank A. Relógio for the HCT116 and Hke3 cell lines. We are grateful to B. Costa-Silva, C. Carvalho, L. Saúde and L. Patton for critically reading the manuscript and J. Escandell and I. P. Castro for helpful discussions. MGF is an International Early Career HHMI scientist.

1 Hidalgo M, Amant F, Biankin A V, Budinská E, Byrne A T, Caldas C, Clarke R, B, de Jong, S, Jonkers J, Maelandsmo G M, et al. (2014) Patient-derived Xenograft models: An emerging platform for translational cancer research. Cancer Discovery, *4*(9), 998–1013. doi.org/10.1-158/2159-8290.CD-14-0001

2 Zon L and Peterson R (2010) The new age of chemical screening in zebrafish. Zebrafish, *7*(1):1. doi: 10.1089zeb.2010.9996.

3 White R, Rose K, and Zon L (2013) Zebrafish cancer: the state of the art and the path forward. Nat Rev Cancer, *13*(9), 624–636. dx.doi.org/10.1038/nrc3589

4 Veinotte C J, Dellaire G, and Berman J N (2014) Hooking the big one: the potential of zebrafish xenotransplantation to reform cancer drug screening in the genomic era. Dis Model Mech, *7*(7), 745–754. doi: 10.1242/dmm.015784

5 Haldi M, Ton C, Seng WL, McGrath P (2006) Human melanoma cells transplanted into zebrafish proliferate, migrate, produce melanin, form masses and stimulate angiogenesis in zebrafish. Angiogenesis.;9(3):139-51. doi: 10.1007/s10456-006-9040-2

6 Marques I, J, Weiss F, U Vlecken, D H Nitsche, C Bakkers J, Lagendijk A K, Partecke L, I Heidecke C D, Lerch M M, Bagowski C P (2009) Metastatic behaviour of primary human tumours in a zebrafish xenotransplantation model. BMC Cancer, *9*, 128. doi: 10.1186/1471-2407-9-128

7 Nicoli S, Ribatti, D, Cotelli F, & Presta M (2007) Mammalian Tumor Xenografts Induce Neovascularization in Zebrafish Embryos. Cancer Research, *67*(7), 2927–2931. doi:10.115-8/0008-5472.CAN-06-4268

8 Zhao C, Wang X, Zhao Y, Li Z, Lin S, Wei Y and Yang H (2011) A novel xenograft model in zebrafish for high-resolution investigating dynamics of neovascularization in tumors. *PLoS ONE*, *6*(7), 1–9. https://doi.org/10.1371/journal.pone.0021768

9 Hewitt R E, McMarlin A, Kleiner D, Wersto R, Martin P, Tsokos M, Stamo G W,Stetler-Stevenson W G (2000) Validation of a model of colon cancer progression. The Journal of Pathology, 192(4), 446–454. DOI:10.1002/1096-9896(2000)9999:9999<::AID-PATH775>3-.0.CO;2-K

10 Shirasawa S, Furuse M, Yokoyama N, and Sasazuki T (1993) Altered growth of human colon cancer cell lines disrupted at activated Ki-ras. Science, *260*(5104), 85–88. doi: 10.1-126/science.8465203

11 Sadanandam A, Lyssiotis C A, Homicsko K, Collisson E A, Gibb W J, Wullschleger S, Ostos L C, Lannon W A, Grotzinger C, Del Rio M et al. (2013) A colorectal cancer classification system that associates cellular phenotype and responses to therapy. Nat Med, *19*(5), 619–625. doi:10.1038nm.3175

12 Hanahan D and Weinberg R A (2011) Hallmarks of cancer: The next generation. Cell, *144*(5), 646–674. doi:10.1016/j.cell.2011.02.013

13 Lawson N D and Weinstein B M (2002) In Vivo Imaging of Embryonic Vascular Development Using Transgenic Zebrafish. Developmental Biology, 248(2), 307–318. https://doi.org/10.100-6/dbio.2002.0711

14 Xiao F, Qiu H, Cui H, Ni X, Li J, Liao W, Lu L, Ding K (2015) MicroRNA-885-3p inhibits the growth of HT-29 colon cancer cell xenografts by disrupting angiogenesis via targeting BMPR1A and blocking BMPSmadId1 signaling. Oncogene 34(15):1968-78. doi: 10.1038/onc.2014.134.

15 Lai K C, Hsu S C, Yang J S, Yu C C, Lein J C and Chung J G (2015) Diallyl trisulfide inhibits migration, invasion and angiogenesis of human colon cancer HT-29 cells and umbilical vein endothelial cells, and suppresses murine xenograft tumour growth. Journal of Cellular and Molecular Medicine, 19(2), 474–484. doi: 10.1111/jcmm.12486

16 Nguyen D X, Bos P D and Massague J (2009) Metastasis: from dissemination to organ-specific colonization. Nat Rev Cancer, *9*(4), 274–284. dx.doi.org10.1038nrc2622

17 Valastyan S1, Weinberg RA. (2011). Tumor metastasis: molecular insights and evolving paradigms. Cell. 2011 Oct 14;147(2):275-92. doi: 10.1016/j.cell.2011.09.024.

18 Stoletov K, Kato H, Zardouzian E, Kelber J, Yang J, Shattil S, and Klemke R (2010) Visualizing extravasation dynamics of metastatic tumor cells. Journal of Cell Science, *123*(Pt 13), 2332–41. doi: 10.1242/jcs.069443

19 Ninomiya I, Terada I, Yoshizumi T, Takino T, Nagai N, Morita A, Fushida S, Nishimura G, Fujimura T, Ohta T and Miwa K (2004) Anti-metastatic effect of capecitabine on human colon cancer xenografts in nude mouse rectum. International Journal of Cancer, *112*: 135–142. doi:10.1002/ijc.20360

20 Van Cutsem E, Cervantes A, Nordlinger B, Arnold D and The ESMO Guidelines Working Group (2014) Metastatic colorectal cancer: ESMO clinical practice guidelines for diagnosis, treatment and follow-up. Annals of Oncology, *25*(April 2002), iii1–iii9. doi: 10.1093/an-nonc/mdu260

21 Colucci G, Gebbia V, Paoletti G, Giuliani F, Caruso M, Gebbia N, Maiello E (2005) Phase III randomized trial of FOLFIRI versus FOLFOX4 in the treatment of advanced colorectal cancer: A Multicenter Study of the Gruppo Oncologico Dell'Italia Meridionale. Journal of Clinical Oncology, *23*(22), 4866–4875. doi.org10.1200JCO.2005.07.113

22 Klampfer L, Swaby LA, Huang J, Sasazuki T, Shirasawa S, Augenlicht L (2005) Oncogenic Ras increases sensitivity of colon cancer cells to 5-FU-induced apoptosis. Oncogene. Jun 2;24(24):3932-41. doi:10.1038/sj.onc.1208552

23 Priego S, Feddi F, Ferrer P, Mena S, Benlloch M, Ortega A, Carretero J, Obrador E, Asensi M, Estrela JM (2008) Natural polyphenols facilitate elimination of HT-29 colorectal cancer xenografts by chemoradiotherapy: a Bcl-2- and superoxide dismutase 2-dependent mechanism. Mol Cancer Ther. 2008 Oct;7(10):3330-42. doi: 10.1158/1535-7163.MCT-08-0363

24 Chen D, Wei L, Yu J and Zhang L (2014) Regorafenib inhibits colorectal tumor growth through PUMA-mediated apoptosis. Clinical Cancer Research: An Official Journal of the American Association for Cancer Research, *20*(13), 3472–3484. doi: 10.1158/1078-0432.C-CR-13-2944

25 Karapetis C S, Khambata-Ford S, Jonker D J, O'Callaghan C J, Tu D, Tebbutt N C, Simes

R J, Chacal H, Shapiro J D, Robitaille S, et al. (2008) KRAS Mutations and Benefit from Cetuximab in Advanced Colorectal Cancer. New England Journal of Medicine, *359*(17), 1757–1765. doi: 10.1056/NEJMoa0804385

26 Van Schaeybroeck S, Kalimutho M, Dunne P D, Carson R, Allen W, Jithesh P V, Redmond K L, Sasazuki T, Shirasawa S, Blayney J, et al. (2014) ADAM17-dependent c-MET-STAT3 signaling mediates resistance to MEK inhibitors in KRAS mutant colorectal cancer. Cell Rep. 2014 Jun 26;7(6):1940-55. doi: 10.1016/j.celrep.2014.05.032

27 De Roock W, Jonker D J, Di Nicolantonio F, Sartore-Bianchi A, Tu D, Siena S, Lamba S, Arena S, Frattini M, Piessevaux H, et al. (2010) Association of kras p.g13d mutation with outcome in patients with chemotherapy-refractory metastatic colorectal cancer treated with cetuximab. JAMA, *304*(16), 1812–1820. doi: 10.1001/jama.2010.1535

28 Iwamoto M, Kawada K, Nakamoto Y, Itatani Y, Inamoto S, Toda K, Kimura H, Sasazuki T, Shirasawa S, Okuyama H, et al. (2014) Regulation of 18F-FDG accumulation in colorectal cancer cells with mutated KRAS. J Nucl Med.Dec;55(12):2038-44. doi: 10.2967jnumed.114-.142927.

29 Grothey A, Van Cutsem E, Sobrero A, Siena S, Falcone A, Ychou M, Humblet Y, Bouché O, Mineur L, Barone C, et al. (2016) Regorafenib monotherapy for previously treated metastatic colorectal cancer (CORRECT): an international, multicentre, randomised, placebo-controlled, phase 3 trial. The Lancet, 381(9863), 303–312. doi.org10.1016S0140-6736(12)61900-X

30 Sato T, Stange D E, Ferrante M, Vries R G, Van Es J H, Van den Brink S, Van Houdt W J, Pronk A, Van Gorp J, Siersema P D, Clevers H (2011) Long-term expansion of epithelial organoids from human colon, adenoma, adenocarcinoma, and Barrett's epithelium. Gastroenterology. 2011 Nov;141(5):1762-72. doi: 10.1053j.gastro.2011.07.050.

31 Fujii M, Shimokawa M, Date S, Takano A, Matano M, Nanki K, Ohta Y, Toshimitsu K, Nakazato Y, Kawasaki K, et al. (2016) A Colorectal Tumor Organoid Library Demonstrates Progressive Loss of Niche Factor Requirements during Tumorigenesis. Cell Stem Cell. 2016 Jun 2;18(6):827-38. doi: 10.1016j.stem.2016.04.003.

32 Guyot F, Faivre J, Manfredi S, Meny B, Bonithon-Kopp C and Bouvier A M (2005) Time trends in the treatment and survival of recurrences from colorectal cancer. Annals of Oncology, 16(5), 756–761. https://doi.org/10.1093/annonc/mdi151

33 André T, Boni C, Mounedji-Boudiaf L, Navarro M, Tabernero J, Hickish T, Topham C, Zaninelli M, Clingan P, Bridgewater J et al. (2004) Oxaliplatin, Fluorouracil, and Leucovorin as Adjuvant Treatment for Colon Cancer. New England Journal of Medicine, 350(23), 2343–2351. https://doi.org/10.1056/NEJMoa032709

34 Hsu H, Thiam T K, Lu Y, Yeh C Y, Tsai W, You J F, Hung H Y, Tsai C-N, Hsu A, Chen H-C et al. (2016) Mutations of KRAS / NRAS / BRAF predict cetuximab resistance in metastatic colorectal cancer patients Patient characteristics, *7*(16). doi: 10.18632/oncotarget.8076

35 Vogelstein B, Papadopoulos N, Velculescu V E, Zhou S, Diaz L A, and Kinzler K W (2013). Cancer Genome Landscapes. Science, *339*(6127), 1546–1558. doi: 10.1126/science.1235122.

36 Almendro V, Marusyk A, and Polyak K (2013) Cellular Heterogeneity and Molecular Evolution in Cancer. Annual Review of Pathology: Mechanisms of Disease, *8*(1), 277–302. doi.org10.1146annurev-pathol-020712-163923

37 Kreso A, O'Brien C A, van Galen P, Gan O I, Notta F, Brown A M, Ng K, Ma J, Wienholds E, Dunant C et al. (2013) Variable Clonal Repopulation Dynamics Influence Chemotherapy Response in Colorectal Cancer. *Science*, *339*(6119), 543–548. doi: 10.1126/science.1227670

38 Bailey AM, Mao Y, Zeng J, Holla V, Johnson A, Brusco L, Chen K, Mendelsohn J, Routbort MJ, Mills GB, Meric-Bernstam F (2014) Implementation of biomarker-driven cancer therapy: existing tools and remaining gaps. Discov Med. 2014 Feb;17(92):101-14.

39 Burstein H J, Mangu P B, Somerfield M R, Schrag, Samson, D, Holt L, Zelman D, Ajani DA (2011) American Society of Clinical Oncology Clinical Practice Guideline Update on the Use of Chemotherapy Sensitivity and Resistance Assays. Journal of Clinical Oncology, 29 (24), 3328–3330. doi.org10.1200JCO.2011.36.0354

40 Montero J, Letai A (2016) Dynamic BH3 profiling-poking cancer cells with a stick. Mol Cell Oncol. 2016 Mar 10;3(3):e1040144. doi: 10.108023723556.2015.1040144.

41 Montero J, Sarosiek K A, Deangelo J D, Maertens O, Ryan J, Ercan D, Piao H, Horowitz N S, Berkowitz R S, Matulonis U, et al. (2015) Drug-Induced death signaling strategy rapidly predicts cancer response to chemotherapy. Cell, 160(5), 977–989. doi.org10.1016j.cell.201-5.01.042

42 Young M, & Reed K R (2016) Organoids as a model for colorectal cancer. *Current Colorectal Cancer Reports*, *12*(5), 281-287. doi:10.1007s11888-016-0335-4

43 Tang Q, Abdelfattah N S, Blackburn J S, Moore J C, Martinez S A, Moore F E, Lobbardi R, Tenente I M, Ignatius M S, Berman J N, et al. (2014) Optimized cell transplantation using adult rag2 mutant zebrafish. Nat Methods. Aug;11(8):821-4. doi: 10.1038/nmeth.3031.

44 Moore J C, Tang Q, Yordán N T, Moore F E, Garcia E G, Lobbardi R, Ramakrishnan A ,Anselmo A, Sadreyev R I, Langenau D M (2016). Single-cell imaging of normal and malignant cell engraftment into optically clear prkdc -null SCID zebrafish. The Journal of Experimental Medicine, 213(12), 2575–2589. https://doi.org/10.1084/jem.20160378